Two-particle element for magnetic memory

D. M. Forrester,[1] Karl E. Kürten,[1,2] and F. V. Kusmartsev[1]
[1]*Department of Physics, Loughborough University, LE11 3TU, United Kingdom*
[2]*Faculty of Physics, University of Vienna, 5, Boltzmanngasse, A-1090 Vienna, Austria*
(Received 24 April 2007; revised manuscript received 8 July 2007; published 9 October 2007)

We propose to use a stack of two or more isolated disk-shaped particles as an element for magnetic memory. Such an element represents a magnetic tunnel junction which is characterized by a few stable states separated by large energy barriers. The switching between the states may be induced by applying a spin-polarized current or a magnetic field. We have described the behavior of the stable states and the associated energies of the stack in magnetic fields. In addition, we have described the magnetizations as well as all possible types of hysteresis loops which such an element may have. We discuss the stability of the information stored in the element and determine a critical magnetic field at which the switching of the element arises.

DOI: 10.1103/PhysRevB.76.134404 PACS number(s): 05.50.+q, 75.10.Hk, 75.75.+a, 75.60.Ch

I. INTRODUCTION

On the one hand, the emerging technology known as spintronics is going to make a step towards the broad use of spin degrees of freedom. On the other hand, the magnetic memory structures have a tendency to be made of smaller and smaller elements. With the ever decreasing scales of these elements comes the necessity to find a greater understanding of their magnetization properties, their responses to applied fields, and their hysteretic characteristics. One form of magnetic memory is magnetoresistive random access memory (MRAM), which uses the magnetic tunnel junction (MTJ) to store information.[1] Within this element the MTJ stack consists of two ferromagnetic layers separated by a thin dielectric barrier. MRAM stores data by utilizing the magnetic polarity of ferromagnetic layers.[2–4] The reading of information is performed by measuring the current, which is determined by the rate of electron quantum tunneling through the MTJ stack. The MTJ resistance is measured across the stack to determine the cell state. Increasing the density of MRAM array cells is only possible by decreasing the size of the MTJ. However, with a small size there are issues such as thermal instability.[5] The critical magnetic field cannot simply be raised because this also generates an increased current flow. In some proposals one uses the thermal heat itself to help to select the cell for writing.[6–8] As a material approaches its Curie point, the critical magnetic field H_c drops, so that less current is needed to write the information.[9] To address the issue a synthetic antiferromagnetic trilayer stack (SAF) has been proposed.[6–8]

Here we propose to use small magnetic disk-shaped particles to build up a MTJ. One of the most simple constructions of MTJs may consist of two monodomain ferromagnets separated by an insulator or normal metal. The monodomain nanodots can be made of NiZn with a diameter of about $d \approx 40$ nm or super-permalloy with a diameter $d \approx 100$ nm and thickness $h \approx 10$ nm. Studies of magnetism at small length scales have been a rapidly growing area of physics. Small magnetic particles and artificial thin-film structures that are based on ferromagnetic or antiferromagnetic layers separated by nonmagnetic spacers are the basic structural elements for an enormous scope of technical applications. Data storage and magnetic sensing are just some of the areas in everyday life where they find uses.[6–8,10]

The giant magnetoresistant (GMR) effect in antiferromagnetically coupled multilayers of the MTJ is in the heart of many specific applications.[11,12] Such nanomagnets can provide the basis for experimental systems that are used to study fundamental phenomena in spintronics. Because of the hierarchy of competing interactions, these many-particle systems display rather rich and interesting collective behavior not found in bulk crystalline magnets. Networks of elementary interacting small magnetic particles, smaller than the bulk domain size, are potential future candidates for MRAM to store and to propagate information. Such new memory may consist of a network or a one-dimensional chain of circular or elliptic pairs of disk-shaped monodomain particles. Chains of circular nanomagnets with diameter less than 100 nm and thickness not more than 10 nm, made from super-permalloy have been studied by Cowburn and Welland.[13] They showed that such chains may be a good means for information processing.

II. REAL SYSTEM AND MODELING OF THE TWO-PARTICLE INTERACTION

Let us now estimate the energy of the magnetostatic interaction of a coupled pair of such disk-shaped particles. These particles are stacked vertically and are similar to those used in the Cowburn-Welland experiments.[13] We assume that such particles have geometries that are of an elliptical disk shape. They have a-semiaxis lengths of 70 nm, b-semiaxis lengths of 35 nm, and thicknesses of 30 nm. We assume that they are separated on the distance of 70 nm as in the Cowburn-Welland experiments.[13] Each particle is acting as a single classical magnetic moment. Let as consider two flat particles—say, two disk ellipses. Then the magnetic moment is within the plane of each particle. When particles are separated far from each other, they are interacting purely as dipoles. At the considered geometry (the stack) the interaction is antiferromagnetic. Such a dipole-dipole interaction is modified (decreases) when the separation distance decreases due to a contribution from higher multipoles. To estimate such a constant of interaction at very small distance between

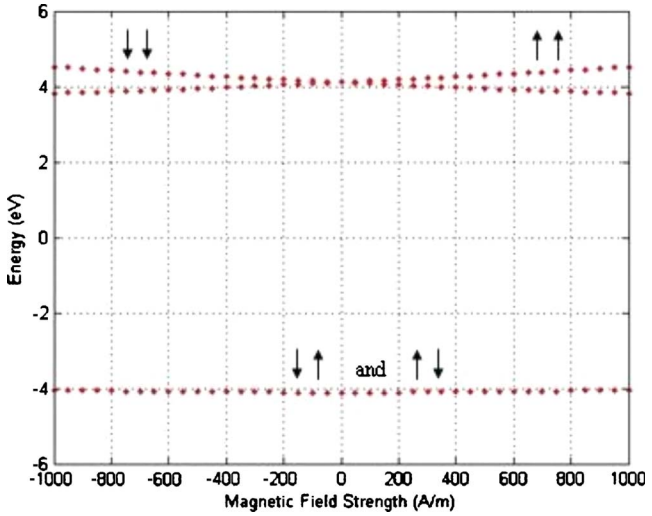

FIG. 1. (Color online) The magnetic energy as a function of magnetic field strength. The arrows next to the curves are indicative of the direction of the magnetizations in each particle in the system; i.e., there are four system orientations represented here. At a field strength equal to zero the difference in the energies of the ground state and the excited level is about 8 eV, giving a value of J_0 of around 4 eV if $S_i = \pm 1$.

the particles we have to do a numerical modeling. For this purpose we use a finite-element method. We model the particles separated by 70 nm in the finite-element package from Comsol using its magnetostatics package. The particles are modelled using a mesh that consists of 12 671 elements. The magnetostatic energy may be estimated with the use of the equation

$$E_m = \frac{\mu_0}{2} \int_{all\ space} H_m^2 dV = -\frac{\mu_0}{2} \int_{body} \mathbf{H}_m \cdot \mathbf{M} dV, \qquad (1)$$

where the value H_m is the magnetic field produced by the magnetic particles and μ_0 is the permeability of free space. It is determined by a solution of the Maxwell equations.[14] The value $\mathbf{M}$ is the magnetization of particles. In an applied field $\mathbf{H}$ we have to include the term

$$E_H = -\mu_0 \int (\mathbf{M} \cdot \mathbf{H}) dV. \qquad (2)$$

Figure 1 is generated from the use of the FEMLAB package to solve the Maxwell equations and examination of the magnetostatic energies within the particles. Since each particle has a shape of the elongated disk, its magnetic moment is directed along this elongation.[15] At zero magnetic field for the stack of two such particles there are four different states. The energies of these states calculated with the use of FEMLAB and indicated by pairs of arrows are schematically presented in Fig. 1. There exists an exact degeneracy of the antiferromagnetically ordered states, as is seen in the lowest ground-state energy of the diagram. There are a further two clear energy levels that exist for pairs of particles that have the same vector alignment of their magnetizations. With no applied magnetic field there are only two energy levels. When the field is switched on the branching from the zero-field state occurs in the upper level. The interaction between the particles can be described by $J_0 S_i S_{i+1}$ where S is the normalized particle spin, $S_i = \pm 1$, and J_0 is the particle spin-spin interaction energy. From Fig. 1 the value of J_0 is around 4 eV.

III. MODEL

Our numerical study indicates that the two magnetic particles can be described by the Hamiltonian of the classic anisotropic Dirac-Heisenberg model (see also Refs. 16 and 17):

$$E = +J \sum_{\langle i,j \rangle} \mathbf{S}_i \cdot \mathbf{S}_j + K \sum_{i=1}^{N} (\mathbf{S}_i \cdot \mathbf{e}_y)^2 - \mathbf{H} \cdot \sum_{i=1}^{N} \mathbf{S}_i, \qquad (3)$$

where the spin operators are substituted by the unit vectors S_i corresponding to the spin on site i. H is the uniform magnetic field applied in a direction of the angle β with respect to the easy axis. The quantity $K > 0$ specifies the strength of the uniaxial anisotropy, while the quantity J describes the strength of the nearest-neighbor interaction. At large separation of particles the constant J comes directly from the dipole-dipole interaction. At small separation distance between particles this constant should be found numerically as we have described in the previous section. We remark that the dipole-dipole interaction inside the particles is neglected, since for small spherical particles this energy contribution is small compared with the contribution from the dominant exchange interactions. The same argument holds for the shape anisotropy such that the anisotropy contribution mainly stems from surface effects. The local energy minima of the system are crucial for the hysteresis effects discussed below. The particles are so small that we may consider them as elementary monodomain units which take the shape of very flat disks. That is, within each particle all the magnetic moments are ferromagnetically aligned. Under these assumptions the preferential orientations of the magnetizations are in-plane and along elongation. There with we can reduce our problem to the study of one-dimensional chains of classical spins associated with these small magnetic particles. We introduce planar polar coordinates $\mathbf{S}_i = (\cos(\phi_i), \sin(\phi_i))$ where the magnetization direction of particle i is described by the variable ϕ_i. Using this with our numerical analysis, given in the previous section, we may write the total energy of the system as the classical two-particle Hamiltonian

$$E = +2J \cos(\phi_1 - \phi_2) + \frac{K}{2}[\sin^2(\phi_1) + \sin^2(\phi_2)] - H[\cos(\phi_1 - \beta) + \cos(\phi_2 - \beta)]. \qquad (4)$$

The quantity β specifies the angle of the external field with the main symmetry axis of the particles (the easy axis). The dynamical behavior of the particles is governed by three competing energy terms, which can give rise to multistability and coexistence of various physical phases. The first term defines the nearest-neighbor interaction, which is effectively associated with the dipole-dipole interaction. The next two

terms are due to the anisotropy. The last two terms specify the Zeeman energy. Since H and K can be scaled by J, we can choose $|J|=1$. According to the variational principle, the extremal points of the Hamiltonian may be determined from the force equilibrium equations

$$\frac{\partial E}{\partial \phi_1} = 2J\sin(\phi_1-\phi_2) + H\sin(\phi_1-\beta) + K\sin(\phi_1)\cos(\phi_1) = 0 \quad (5)$$

and

$$\frac{\partial E}{\partial \phi_2} = 2J\sin(\phi_2-\phi_1) + H\sin(\phi_2-\beta) + K\sin(\phi_2)\cos(\phi_2) = 0. \quad (6)$$

The stability and the character of these extremal points may be determined with the use of the Hessian matrix

$$N_{\text{Hessian}} = \begin{bmatrix} \frac{\partial^2 E}{\partial \phi_1^2} & \frac{\partial^2 E}{\partial \phi_1 \phi_2} \\ \frac{\partial^2 E}{\partial \phi_2 \phi_1} & \frac{\partial^2 E}{\partial \phi_2^2} \end{bmatrix}. \quad (7)$$

After finding the solution of Eqs. (5) and (6) we have to determine the sign of the determinant of the Hessian matrix. If this value is positive, then the found solution is associated with local minima (or maxima) and therefore it is stable (or unstable) or metastable. The separation of the absolute minima and maxima is made with the use of the sign of the first eigenvalue. However, if the determinant of the Hessian matrix is negative, then the found solution is associated with saddle points and therefore it is unstable. Therefore the stability criterion is determined by zeros of the determinant of the Hessian matrix.

IV. GENERIC STATE DIAGRAM AT ARBITRARY MAGNETIC FIELD

The type of ground state of the considered system of two particles depends both on the amplitude and direction of the applied magnetic field as well as on the value of the anisotropy K. Generically such a state cannot only be of the classical ferromagnetic and antiferromagnetic type. Here there may arise the state when the magnetic moments of these two particles are oriented at some angle with respect to each other. Obviously at large magnetic fields these moments must align in the direction of the field. Here we find a realization of two ferromagnetic states $\mathbf{F}^{\uparrow\uparrow}$ and $\mathbf{F}^{\downarrow\downarrow}$ specified by the angles $x_1=x_2\approx\beta$ and $x_1=x_2\approx\pi+\beta$, respectively, provided that the magnitude of the magnetic field is strong enough and the field is oriented at the angle β with respect to the main axis of the anisotropy. For $\beta=0$ the corresponding energies are $E_F=2-2H$ and $E_F=2+2H$, respectively. The stability of one or other of these states will depend on the history—i.e., from which field and from which state the present state has been originated. This subtle issue of the system behavior is related to the formation of the hysteresis loop which will be discussed in the next section. If the field

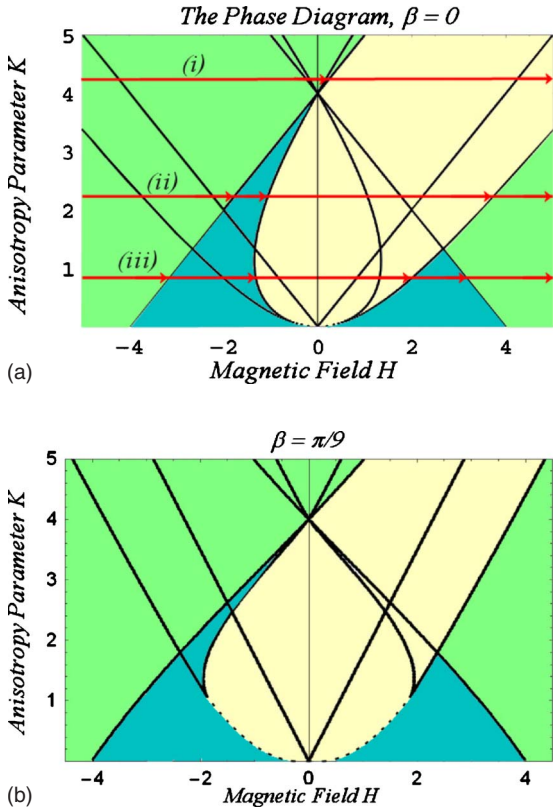

FIG. 2. (Color online) Diagrams of different states existing in a magnetic tunnel junction which arise with an increasing external magnetic field. The field is applied in the plane parallel to the main axis of anisotropy. The original antiferromagnetic orientation of the particles and their shape are associated with the parameter K. Large positive values of K indicate that the monodomain particles are strongly elongated along the X direction. These phase diagrams are obtained when we start from large positive or negative values of magnetic field. The diagrams of the states associated with the case of decreasing magnetic field may be obtained by a simple reflection.

decreases from the original very large positive or negative value, these two ferromagnetic states $\mathbf{F}^{\uparrow\uparrow}$ or $\mathbf{F}^{\downarrow\downarrow}$ are stable when $H>4-K$ or $H<K-4$, respectively (see Fig. 2).

The transitions between different states when the magnetic field increases from ∞ are presented in the Fig. 2(a). For an illustration we have chosen the case when an applied magnetic field directed at an angle $\beta=0$. The arrows along lines (i), (ii), and (iii) of this diagram correspond to the anisotropy parameters equal to 1, 2.1, and 4.3, respectively. Each arrow indicates the point on lines (i), (ii), and (iii) when an appropriate phase becomes unstable. The coloring in the diagram indicates the range of the existence for a particular phase. The lightest shade (light yellow online) is used to depict the antiferromagnetic alignment. Those areas of an intermediate hue (green online) are areas in the (H, K) plane where a ferromagnetic state exists. The darkest coloring (blue online) is for cases exhibiting a scissored or canted state. Thus the points highlighted by arrows indicate the values of magnetic field where there is a change in the system magnetization characteristics. That is, there a transition between a ferromagnetic to antiferromagnetic or to a scissored

states occurs. These points will be elaborated upon in the following discussion involving the related hysteresis loops of magnetization against the magnetic field. Figure 2(b) carries the same information as for $\beta=0$, but is for $\beta=\pi/9$. Again the critical points in the (H, K) plane is where there are intermediate lines separated by differing shades (color online).

For $\beta=0$, we further find the antiferromagnetic (AF) state characterized by the angles $(\phi_1,\phi_2)=(0,\pi)$ and $(\phi_1,\phi_2)=(\pi,0)$ with the corresponding constant energy $E_{AF}=-2$. This can be realized at a small magnetic field. Again, for the ferromagnetic states the stability will depend on the history. Finally there exists a scissored phase (SC) specified by the angle relation $\phi_1=-\phi_2$ with $\phi_1=\arccos[H/(4-K)]$. Note that this state is often referred to as the spin-flop "phase."[18] The corresponding energy takes the value $E_{SC}=(K-2)-H^2/(4-K)$.

In Fig. 2(a), above $K=4$, there is no SC state and there are only transitions between F and AF states. At $K=4.3$, indicated by the line in Fig. 2(a) labeled by (i), a transition from $F^{\downarrow\downarrow}$ to AF occurs with $H=K-4=0.3$. This state is held until $H=\sqrt{K(4+K)}=5.97$ where the system becomes $F^{\uparrow\uparrow}$.

The level of anisotropy identified at (ii) in Fig. 2(a) is $K=2.3$. There comes a point where the transition from a ferromagnetic (intermediate color) to a scissored state (dark color) occurs. The bold line in the diagram that marks this is given by $H=K-4=-1.7$. Upon exiting the scissored state an antiferromagnetic status comes about. This occurs along the line $H=(K-4)\sqrt{K/(4+K)}=-1.03$. The next critical line is associated with the transition from an antiferromagnetic to a ferromagnetic state. The equation of the line is $H=\sqrt{K(4+K)}=3.8$.

We now describe the transitions arising along the line in Fig. 2(a) at $K=0.8$ indicated by (iii). As the field has a large negative starting value, this means that the system begins life in the $F^{\downarrow\downarrow}$ state. This state is shown in the diagram through the use of the midtone coloring (green online). There comes a point, when following the arrows at level (iii), that a transition into $SC^{\swarrow\searrow}$ is made. This occurs at $H=K-4=-3.2$ and takes us into the dark area (blue online) in the negative half of the diagram. Continuing along the line (iii) brings us into the AF state at $H=-1.31$ [lightest area in Fig. 2(a), light yellow online]. Again, slowly increasing the field we hit the point where $H=1.96$ and $SC^{\nwarrow\nearrow}$ is generated. Finally, when the field reaches $H=3.2$ the emergence of the $F^{\uparrow\uparrow}$ state from the $SC^{\nwarrow\nearrow}$ state occurs.

In the state diagram presented in Fig. 2 there are regions where there may coexist more than one different state. We have the triple points $(H,K)=(\pm\frac{8}{3},\frac{4}{3})$ where each of the three phases described above may exist. At the value $(H,K)=(0,4)$ all (four) phases may coexist. These critical points will be decisive in the next discussion in order to give a proper classification to all the possible hysteresis loops. The evolution of the two magnetization angles ϕ_1 and ϕ_2 as a function of the magnetic field, for an anisotropy strength below the critical point $K=\frac{4}{3}$, is illustrated in Fig. 3.

We start from ∞ and decrease the field slowly. Within Fig. 3 the first transition occurs when the $F^{\uparrow\uparrow}$ phase reaches instablility and becomes $SC^{\nwarrow\nearrow}$ at $(H,K)=(3,1)$. This is a

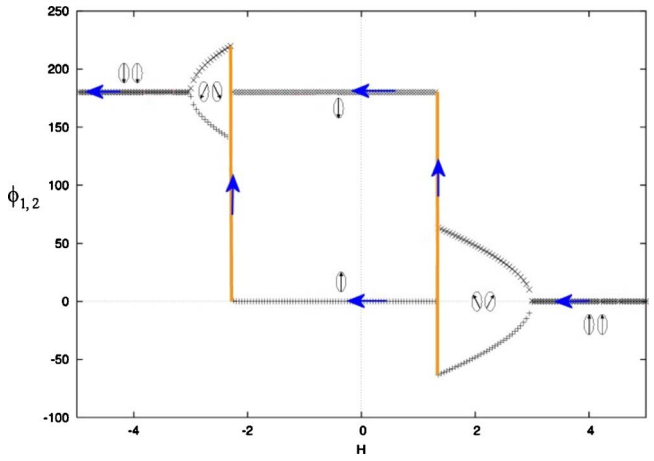

FIG. 3. (Color online) The magnetization angles of the two particles as a function of magnetic field and anisotropy parameter $K=1$. Here the magnetic field is going from a positive value downwards into the negative range.

smooth transition in the form of a pitchfork bifurcation. This state persists until the point in Fig. 3 where the field is $H=1.34$ and the AF state begins. The AF state is seen to become $SC^{\swarrow\searrow}$ at $H=-\sqrt{5}$. This state ends when $H=K-4=-3$, and the complementary ferromagnetic state $F^{\downarrow\downarrow}$ is emerged continuously.

When the magnetic field is not aligned with the main axis of anisotropy there arises a state $\mathbf{AF}^{\uparrow\downarrow}$ characterized by the angles close to $(\phi_1,\phi_2)=(0,\pi)$. We call such a state as an approximately antiferromagnetic state. Only for $\beta=0$ these two angles are associated with antiparallel spin alignment—i.e., exactly equal to $(0,\pi)$. Note also that for $\beta\neq 0$ the magnetic moments of the particles are strictly antiparallel only for zero magnetic field. Eventually there exists a so-called scissored phase $\mathbf{CS}^{\swarrow\searrow}$ whose onset is characterized by a pitchfork bifurcation of the two ferromagnetic angles. For $\beta=0$ we have the critical point $H_c=4-K$ and the two branches specified by $\phi_1=\arccos\frac{H}{4-K}$ and $\phi_2=-\arccos\frac{H}{4-K}$ "scissored" around $\beta=0$. For $K=0$ and arbitrary β the solution of the variational equations (5) and (6) yields, for the two angles "scissored" around the angle β, $\phi_1=\beta+\arccos\frac{H}{4}$ and $\phi_2=\beta-\arccos\frac{H}{4}$.

Below, Figs. 4–6 show the corresponding evolution of the hysteresis loops for $\beta=0$, which can also be extracted completely from our phase diagram depicted in Fig. 2. We stress that a complete classification of all possible hysteresis curves is of fundamental importance in any kind of technical application. Moreover, in the same manner, the qualitative behavior of all possible magnetoresistance curves can directly be extracted from the phase diagrams.

V. PHASE DIAGRAM AND HYSTERESIS LOOPS

Now let us discuss the appearance and type of the hysteresis loops in terms of the magnetisation behavior when the magnetic field changes and their correspondence to the phase diagrams presented in Fig. 2. According to the phase dia-

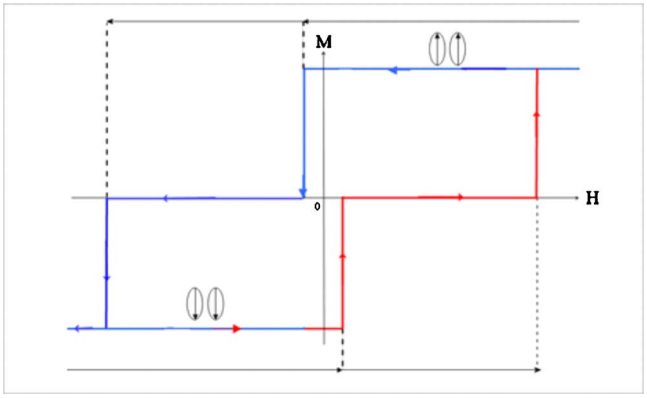

FIG. 4. (Color online) The total magnetization as a function of applied magnetic field strength. This hysteresis curve is illustrative of the process highlighted in Fig. 2(a) at level (i). The arrows below the curve are those imported from Fig. 2(a) at this level of anisotropy ($K=4.3$), marking the transition between the flipped states of the ferromagnetic alignments. When following this line in the direction of the arrows, in Fig. 2(a), a jump occurs at $H=0.29$ from $\downarrow\downarrow$ to AF. The system then holds its orientation in the antiferromagnetic alignment until the magnetic field reaches the value $H=5.97$ where it becomes ferromagnetic again, where the both spins are flipped, $\uparrow\uparrow$.

gram, for $K>4$, we only have transitions from the ferromagnetic phase $F^{\uparrow\uparrow}$ through the AF phase to the complementary ferromagnetic $F^{\downarrow\downarrow}$ phase and vice versa.

The orientation of the magnetization is shown in Figs. 4–6 as the magnetic field is successively lowered and heightened through negative and positive values. The field is directed in parallel to the easy axes of the single-domain par-

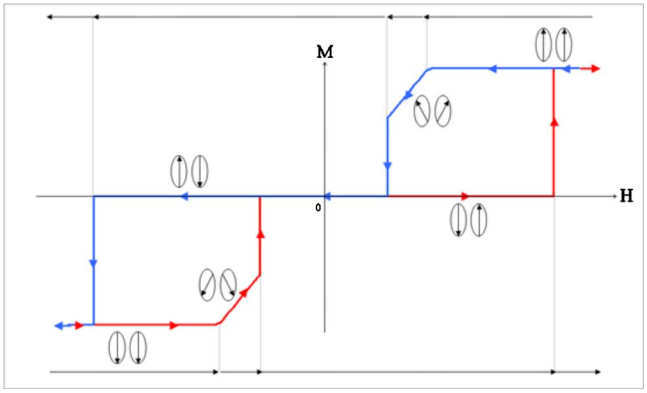

FIG. 5. (Color online) The total magnetization as a function of applied magnetic field strength. This hysteresis curve is illustrative of the process highlighted in Fig. 2 at level (ii) of the anisotropy ($K=2.3$). The arrows below the curve are those seen in Fig. 2(a) at this level, marking the transition between the different alignments. Those above the hysteresis curve are those for the reversal of the magnetic field. Looking at the forward evolution of the magnetic field from a negative applied magnetic field, the transition from $\downarrow\downarrow$ to $\swarrow\searrow$ happens at around $H=1.71$ before jumping to the antiferromagnetic alignment at $H=-1.03$. This state persists until $H=3.8$ where the critical point is found where the jump into $\uparrow\uparrow$ occurs. The reveral of the field gives the inverse mirror image of this evolution.

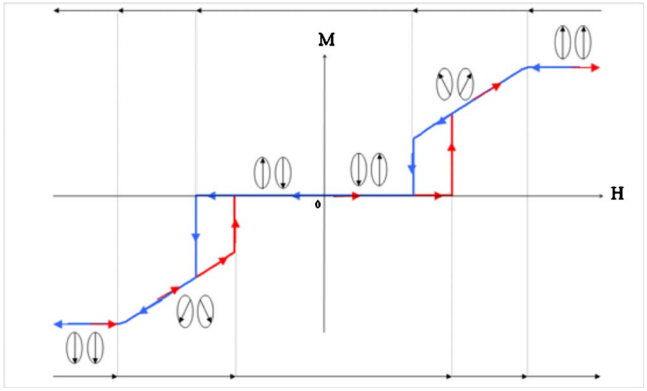

FIG. 6. (Color online) The total magnetization as a function of applied magnetic field strength. This hysteresis curve is illustrative of the process highlighted in Fig. 2 at level (iii) of the anisotropy ($K=0.8$). The arrows below the curve are those imported from Fig. 2(a) at this level, marking the transition between the different alignments. Those above the hysteresis curve are those for the reversal of the magnetic field. Looking at the forward evolution of the magnetic field from a negative applied magnetic field, the transition from $\downarrow\downarrow$ to $\swarrow\searrow$ happens at around $H=-3.21$ before jumping to the antiferromagnetic alignment at $H=-1.31$. This state persists until $H=1.95$ where the critical point is found where the jump to $\nwarrow\nearrow$ occurs. When the field becomes strong enough at $H=3.21$ the transition to $\uparrow\uparrow$ happens. The reveral of the field gives the inverse mirror image of this evolution.

ticles. In Fig. 2 there is a level of anisotropy, $K/J>4$, where the transition between the ferromagnetically ordered states $\uparrow\uparrow$ and $\downarrow\downarrow$ is seen. For one such value of $K=4.3$, as presented in Fig. 2(a), the transition is mapped out by the progression of linear arrows across the diagram and is depicted by (i). In the Fig. 4 we present the hysteresis curve arising at the anisotropy constant $K=4.3$, which is associated with transitions depicted along line (i) in Fig. 2(a). As the value H increases the system remains in the $\downarrow\downarrow$ orientation until a critical point where a jump is made to the AF state. This persists until the field is strong enough to take the system into the $\uparrow\uparrow$ state. Conversely, when the field is in turn lowered progressively the critical level is reached at a point which mirrors that of the preceding evolution and a jump is made from $\uparrow\uparrow$ to $\downarrow\downarrow$. For a value of K at level (ii) in the diagram (see Fig. 4) there is the addition of scissor states—e.g., $\swarrow\searrow$—and antiferromagnetically ordered ones. Traversing [see Fig. 2(a)] the line along (ii) the ferromagnetic ordering persists until a level of field where a scissors state begins to emerge. The scissors state is related to splaying the magnetization directions of particles outward from an imaginary central axis. The splaying begins moderately but as the field comes from the low negative strength upwards the overall angle between the magnetization vectors increases. This continues until a critical point where one particle aligns itself with the field and the other becomes the very antithesis of the first. This point is marked by a jump up to zero magnetization in Fig. 5. Increasing the field out of the negative regime, through zero and up to a juncture in the magnetization characteristics where the moments align themselves ferromagnetically upwards in the positive field, the final jump in the forward

evolution is seen. This will happen when the field wins out against all other opposing factors and flips both particles under its influence and into its orientation. Beginning the reduction of the field reverses the process in a manner that gives a negative reflection of the magnetization. The hysteresis curve in Fig. 5 is now attained.

With H equal to zero, and until a point in the field strength where anisotropy no longer holds sway, the system is in an artificial antiferromagnetically ordered state with a moderate level of anisotropy K. The final hysteresis curve described here for $\beta=0$ (Fig. 6) has the lowest level of uniaxial anisotropy and as such is the one with the smallest return loops and greatest propensity for its moments to fluctuate. Beginning with low negative field strength the system starts in its ferromagnetic alignment in harmony with the direction of the field. This saturated magnetization state ends earlier than for higher values of K and a scissors state propagates. This state lasts over a greater range of the magnetic field in this softer material than in the other two hysteresis curves before jumping to the antiferromagnetic distribution. Antiferromagnetism between the particles is maintained until the jump to a new scissors state is made at another critical level of applied field strength. These new scissors begin to close as the field comes to dictate more until they become parallel and the complete flip of both particles has arrived. Upon reversing the magnetic fields cycle the hysteresis curve is born, showing smaller hysteresis and consequentially less energy loss than its predecessors. The material featuring in this kind of curve is one that has a more rapid response to the field and a small remanence. The particles magnetizations align opposite to one another with zero H due to the demagnetization fields or rather the fields arising from the magnetic poles at the edges of the elliptical particles.

Now let is discuss the evolution of the hysteresis curves when the magnetic field is applied at some angle β to the main axis of the symmetry of the discussed ellipses. For a low value of anisotropy, such as $K=0.5$, there exists no hysteresis. When considering the system to start in the negative field it begins with ferromagnetic alignment of the two particles. At a value of magnetic field, $H=-3.61$, the first-order transition to a canted state begins and continues smoothly into an antiferromagnetic arrangement. The reversal of this magnetic field creates the exact reproduction of the path followed by the forwards evolution. Figure 7 shows the evolution of the magnetization as a function of a magnetic field H applied at an angle of $\beta=\pi/9$ with $K=2.1$. Again, starting with a negative field, ferromagnetism is maintained between the particles until the transition is made to a scissored orientation at $H=-2.06$. The angle between the magnetization directions increases as the field does until there is a critical point at which a jump into antiferromagnetic alignment occurs. This happens at $H=-1.69$. The antiferromagnetic state is held but as the field approaches the value $H=2.57$ it begins to alter into a weakly scissored state that is almost an antiferromagnetic one. At $H=2.57$ another jump is seen which leads straight to the ferromagnetic state that is opposite to the one in which the system began. Hysteresis is seen in this example, and upon reversing the field the inverted mirror image of the forwards branch is seen. Figure 7 demonstrates the stabilities in the system which are determined by zeros of

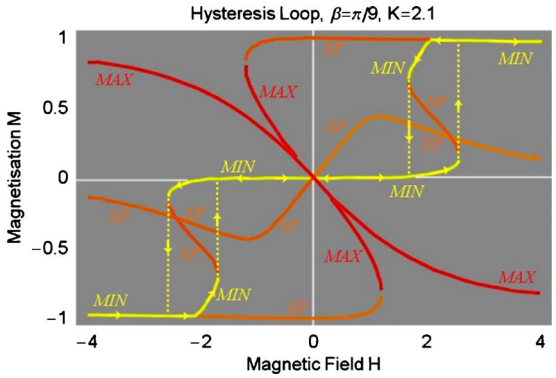

FIG. 7. (Color online) The field is cycled from a negative value and back with the arrows indicating the direction of evolution throughout the system. Here $K=2.1$. The stable minima are shown as the lightest color (yellow online) and the description "Min," the saddle points as an intermediate colour (orange online) and the description "SP," and the maxima by the darkest shade (red online) and the description "Max."

the determinant of the Hessian matrix. With magnetic field changes the system evolves through the stable minima of the energy landscape. These minima are presented by the lines of the lightest color in the figure (yellow online). Also in the figure the saddle points and maxima are represented in darker colors. In this figure the saddle points of the energy landscape correspond to the lines of intermediate shading (orange online), while the maxima of the energy landscape correspond to darker shading (red online). These minima and saddle points are important aspects of the system description. The saddle points may be important for a description of quantum tunneling which unavoidably will arise when the size of the particles decreases. If the interaction between particles changes sign, the minima will be transformed into maxima and vice versa; therefore, we also present evolution of the maxima in a magnetic field.

Figure 8 is for $K=4.3$ in which the system begins in a ferromagnetic state at low negative magnetic field until $H=0.31$ where it jumps to antiferromagnetic. This lasts until

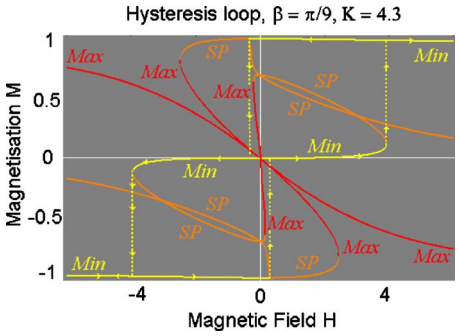

FIG. 8. (Color online) The hysteresis curve for $K=4.3$ is indicated by the direction of the arrows through the stable minima. The stable minima are shown as the lightest color (yellow online) and the description "Min," the saddle points as an intermediate color (orange online) and the description "SP," and the maxima by the darkest shade (red online) and the description "Max."

the magnetic field is strong enough at $H=3.94$ to take the system into a leap up to the magnetization corresponding to the ferromagnetic regime. Again the reversal of the field gives us hystersis but with much larger areas between the branches. It is to be noted that if the system were to have begun in the antiferromagnetic orientation—for example, at $H=0$—then the region between $0<H<0.31$ would have been part of the curve as the field was increased from this orientation. Starting with the system settled in the ferromagnetic area avoids this part of the magnetisation diagram as ferromagnetism is maintained beyond this. Given a specific input value of H the system exists in one of several possible regimes and the input history will dictate which of these is established. For the various levels of anisotropy the system has a complicated structure with many local minima that correspond to metastable states. The minima, maxima, and saddle points are depicted in Fig. 8 in the same manner as in Fig. 7. The data contained in Figs. 7 and 8 are the result of the numerical solution of Eqs. (5) and (6). To determine whether the solutions are minima, maxima, or saddle points the Hessian matrix of Eq. (7) was looked at. When the determinant of the Hessian is greater than zero and the first element (or eigenvalue) of the Hessian matrix is also greater than zero, then there are stable minima. When the first element is less than zero, but the determinant is greater than zero, there are unstable maxima. The solutions that correspond to saddle points are those where the determinant is less than zero.

VI. SUMMARY

We studied the properties of two interacting magnetic particles subjected to exchange interaction J, anisotropy parameter K, and an external magnetic field H with an arbitrary angle β with respect to the easy axis. We further present a complete theoretical study of magnetic phase diagrams as a function of the field for arbitrary strengths of the anisotropy. We classify all possible magnetic hysteresis loops and show the dependence of the corresponding magnetic moments on the external field. These studies can give answers to the problem of finding adequate materials for practical applications such as sensor, storing, or recording devices. We remark that for a larger number of particles the problem of multistability is highly complex and can lead to fractal properties being seen in all the physical variables.[19]

In conclusion, we have demonstrated the behavior of MTJs that are under the influence of an external magnetic field. These MTJs consist of a pair of disk-shaped monodomain particles separated by an insulator. We have studied the stability of the MTJ states and a hysteresis loop both analytically and numerically and made a detailed analysis of the possible hysteresis loops of the proposed MTJs. We have determined a state diagram in the magnetic-field—shape anisotropy plane.

The proposed MTJ may entail a range of applications. Development of new magnetoelectronic devices is probable, and innovations in information processing and THz technology can be anticipated. The possible applications may include models for MRAM constructions and logic gates made from small magnetic particles or their pairs. Novel magnetoelectronic devices may be embraced by memory cells for storing binary data and even a construction for logic gates.[20–25] Many interconnected transmission lines made of MTJs can be designed into networks—nano-MTJ networks which may operate similar to a neural network. A lot of attention has recently been focused on a new class of smart materials that exhibit highly unusual electromagnetic properties associated with negative permeability and refractive index.[26] Normally such materials are made of an array of single or coupled pairs of quantum dots or split ring resonators. On the basis of the studies of the energy landscape of the single MTJ described in the present paper we suggest that arrays of MTJs may have properties similar to those found in the Ref. 26. Therefore these systems may be also considered as smart materials and therefore deserve special attention. Moreover, the high-frequency magnetization reversal of the discussed pair of magnetic particles may be used for a construction of detectors of THz radiation. The design of artificially structured electromagnetic materials that can exploit the frequencies in the THz range is a developing area of science. Magnetic metamaterials are good candidates to produce terahertz devices.[27] These future considerations may lead to the next development of a novel hardware and a new technology based on the nano-MTJs.

ACKNOWLEDGMENT

This work has been supported by the European Science Foundation (ESF) in the framework of the network program "Arrays of Quantum Dots and Josephson Junctions."

[1] J. Daughton, Thin Solid Films **216**, 168 (1992).
[2] J. Akerman, Science **308**, 508 (2005).
[3] John Mallinson, *Magneto-Resistive and Spin Valve Heads* (Academic Press, London, 2002).
[4] E. Hirota, H. Sakakima, and K. Inomata *Giant Magneto-Resistance Devices* (Springer, Berlin, 2002).
[5] J. M. Slaughter *et al.*, JOM-e 52 (2000), www.tms.org/pubs/journals/jom/0006/slaughter/slaughter-0006.html
[6] M. Durlam *et al.* (unpublished).
[7] M. Durlam *et al.*, in *Proceedings of the IEEE International Conference on Integrated Circuit Design and Technology*, edited by D. Jiles (IEEE, New York, 2004).
[8] A. V. Pohm *et al.*, IEEE Trans. Magn. **33**, 3280 (1999).
[9] J. M. Daughton, J. Appl. Phys. **81**, 3758 (1997).
[10] *Magnetic Multilayers and Giant Magnetoresistance*, edited by Uwe Hartmann (Springer, Berlin, 2000).
[11] M. A. Howson, Contemp. Phys. **35**, 347 (1994).
[12] P. Grünberg, Phys. Today **54**(5), 31 (2001).
[13] R. P. Cowburn and M. E. Welland, Science **287**, 1466 (2000).
[14] J. D. Jackson, *Classical Electrodynamics* (Wiley, New York,

1999), pp. 178–199.
[15] P. Vavassori, M. Grimsditch, V. Novosad, V. Metlushko, and B. Illic, Phys. Rev. B **67**, 134429 (2003).
[16] D. M. Forrester, K. E. Kuerten, and F. V. Kusmartsev, Phys. Rev. B **75**, 014416 (2007).
[17] D. Suess, T. Schrefl, W. Scholz, and J. Fidler, J. Magn. Magn. Mater. **242-245**, 426 (2002).
[18] C. Micheletti, R. B. Griffiths, and J. M. Yeomans, Phys. Rev. B **59**, 6239 (1999).
[19] K. E. Kürten and F. V. Kusmartsev, Phys. Rev. B **72**, 014433 (2005).
[20] D. C. Worledge, Appl. Phys. Lett. **84**, 2847 (2004).
[21] Z. Szabo and A. Ivanyi, J. Magn. Magn. Mater. **215-216**, 33 (2000).
[22] R. P. Cowburn, Science **311**, 183 (2006).
[23] James M. Daughton, *Advanced MRAM Concepts* (NVE Corporation, Eden Prairie, 2001).
[24] J. M. Slaughter *et al.*, J. Supercond. **15**, 19 (2002).
[25] K. E. Kürten, *Condensed Matter Theories* (Nova Science, New York, 2006), Vol. 21.
[26] A. N. Grigorenko, A. K. Geim, H. F. Gleeson, Y. Zhang, A. A. Firsov, I. Y. Khrushchev, and J. Petrovic, Nature (London) **438**, 335 (2005).
[27] Hou-Tong Chen *et al.*, Nature (London) **444**, 597 (2006).